Applied Geochemistry 73 (2016) 132–141

Contents lists available at ScienceDirect

Applied Geochemistry

journal homepage: www.elsevier.com/locate/apgeochem

Organic carbon source tracing and DIC fertilization effect in the Pearl River: Insights from lipid biomarker and geochemical analysis

Mingxing Yang, Zaihua Liu*, Hailong Sun, Rui Yang, Bo Chen

State Key Laboratory of Environmental Geochemistry, Institute of Geochemistry, Chinese Academy of Sciences, Guiyang 550081, China

ARTICLE INFO

Article history:
Received 9 May 2016
Received in revised form
9 August 2016
Accepted 13 August 2016
Available online 17 August 2016

Keywords:
Lipid biomarker
Carbon source
Carbonate weathering
In-river primary production
Missing carbon sink
DIC fertilization effect
Pearl River

ABSTRACT

The photosynthetic conversion of dissolved inorganic carbon (DIC) into organic carbon (OC) by using aquatic phototrophs in rivers may serve as a potential carbon sink, especially in the carbonate rock areas, thereby offering a clue for finding the missing carbon sink. However, primary-produced autochthonous OC is erroneously considered as terrestrial-derived allochthonous OC. Thus, carbonate weathering-related carbon sink is underestimated if only DIC concentrations sampled at river mouths are considered, and the transformation of DIC to autochthonous OC is neglected. Therefore, distinguishing sources of autochthonous and allochthonous OC is vital in the assessment of carbon sink. In this study, source-specific biomarkers, in association with chemical compositions and phytoplankton proxies in water samples collected from the Pearl River, were analyzed to determine OC sources. Results showed that biomarkers in the Pearl River were quite abundant, and the calculated average autochthonous OC was approximately 65% of the total OC, indicating intense in-river primary productivity. Moreover, phytoplankton biomass and DIC concentration were positively related, indicating the DIC fertilization effect on aquatic photosynthesis. High total suspended solid (TSS) on the water surface blocked the sunlight and then reduced phytoplankton production. However, in situ photosynthesis of phytoplankton could also produce autochthonous OC, even larger than the allochthonous source at sites with high DIC, and even with higher TSS concentrations. These findings comprehensively elucidated the formation of autochthonous OC based on the coupling action of rock weathering and photosynthetic activity in the riverine system, suggesting a potential direction for finding the missing carbon sink.

© 2016 Elsevier Ltd. All rights reserved.

1. Introduction

Accurate assessment of carbon budget in nature is one of the major prerequisites of global warming studies (Houghton, 2007; Giering et al., 2014; Poulter et al., 2014). However, the 2.8 Pg C/a residual terrestrial carbon sink remains a challenge to comprehensively understand the processes that control the carbon cycle and accurately predict variation in the atmospheric temperature (Melnikov and O'Neill, 2006). Thus, exploring the residual terrestrial carbon sink has emerged as the priority issue in global warming. Rock weathering, especially carbonate weathering, can consume atmospheric CO_2 and hence produce carbon sink (Liu and Zhao, 2000; Gombert, 2002; Liu et al., 2010, 2011; Liu and Wolfgang, 2015). However, whether calcite deposition will release CO_2 back into the atmosphere and cause no net carbon sequestration during karst processes remain ambiguous. Hence, traditional carbon budget models may underestimate carbonate weathering-related carbon sink (Meybeck, 1993). Numerous studies have proved that DIC (dissolved inorganic carbon, including CO_2(aq), HCO_3^-, CO_3^{2-}, mainly HCO_3^- at pH = 7–9) can be preserved in the relatively stable form of organic carbon (OC) through photosynthesis of phytoplankton in aquatic ecosystems (ocean, river, lake, etc.) (Einsele et al., 2001; Cole et al., 2007; Montety et al., 2011; Nimick et al., 2011). Liu et al. presented a H_2O–carbonate–CO_2–aquatic phototroph interaction model, which showed that carbonate weathering could contribute to the long-term carbon sink as sedimentary organic carbon according to the following equation (Liu et al., 2010, 2011; Liu and Wolfgang, 2015):

$$H_2O + CaCO_3 + CO_2 \rightarrow Ca^{2+} + 2HCO_3^- \xrightarrow{\text{Aquatic photosynthesis}} CaCO_3 + x(CO_2 + H_2O) + (1-x)(CH_2O + O_2). \quad (1)$$

* Corresponding author.
E-mail address: liuzaihua@vip.gyig.ac.cn (Z. Liu).

http://dx.doi.org/10.1016/j.apgeochem.2016.08.008
0883-2927/© 2016 Elsevier Ltd. All rights reserved.

The key mechanism of this model lies in the transformation of DIC into OC by aquatic phototrophs, which produces autochthonous OC that is different from terrestrial allochthonous OC. These two types of OC represent the internal and external boundaries of an aquatic system, respectively.

Autochthonous OC is generally derived from primary production caused by aquatic photosynthetic uptake of DIC, whereas allochthonous OC represents terrigenous source such as vascular plant tissues and detritus from marshes and upland sources (Bianchi, 2007; O'Reilly et al., 2014). However, the ratios of autochthonous and allochthonous OCs are quite difficult to determine because of their mixing. Autochthonous OC is often mistakenly regarded as allochthonous OC, resulting in the underestimation of carbonate weathering-related carbon sink. Therefore, distinguishing sources of autochthonous and allochthonous OC is crucial for carbon sink assessment.

Several methods, such as elemental analysis (C/N ratios), isotopic ($\delta^{13}C$) composition, and chemical biomarker methods, have been employed to distinguish the OC sources in aquatic ecosystems. C/N ratios are used to infer algal and vascular plant sources (Meyers, 1997). Generally, C/N ratios for vascular plants (>17) and microalgae (5–7) largely differ based on the structural components. However, C/N ratios are highly variable and influenced by remineralization and decomposition processes, which result in the misidentification of OC sources (Bianchi and Canuel, 2011). Stable isotopes have been used to evaluate sources of particulate and dissolved organic matter (Raymond and Bauer, 2001; Gordon and Goñi, 2003; McCallister et al., 2004) in aquatic ecosystems. However, identifying organic matter sources is difficult when using single isotope in complex systems because of the overlaps in the stable isotopic signatures of source materials (Cloern et al., 2002).

By contrast, lipid biomarkers comprise a group of natural molecules that store energy and act as structural components of cell membranes. Different lipid compositions are associated with diverse biosynthesis pathways (Guschina and Harwood, 2013; Mohanty et al., 2013). Hence, lipid biomarkers with distinct structural features (number and position of double bonds, functional group composition, etc.) can provide source-specific information. These biomarkers have been extensively used in studies that elucidated organic matter sources in aquatic systems (Yunker et al., 1995; Waterson and Canuel, 2008; Tue et al., 2012).

Fatty acids represent a significant fraction of total lipid and have been widely used to trace sources of organic matter (Dalsgaard et al., 2003; Burns et al., 2008; Rontani, 2008). Long-chain saturated fatty acids are generally inferred to indicate terrestrial organic sources (vascular plants), whereas short-chain saturated fatty acids can be derived from aquatic sources (algal and microbial). Monounsaturated fatty acids (MUFA) indicate the presence of fresh algal sources, such as C16:1ω and C18:1ω (Dunstan et al., 1993b). Higher plant sources of polyunsaturated fatty acids (PUFA) are generally represented by C18:2ω and C18:3ω (Harwood and Russell, 1984).

Sterol, which is a group of cyclic alcohols, is another commonly used biomarker (Conte et al., 1995). Terrestrial plants are abundant in 24-ethylcholest-5-en-3β-ol (sitosterol) ($29\Delta^5$) and 24-methylcholest-5-en-3β-ol (campesterol) ($28\Delta^5$) sterols. 24α-methylcholesta-5,22*E*-dien-3β-ol (*epi*-brassicasterol) ($28\Delta^{5,22}$) is particularly contained in phytoplankton (especially diatoms) (Volkman, 1986; Jaffé et al., 1995). Other phytoplankton markers are dinoflagellates and 24-methylcholesta-5,24(28)-dien-3β-ol (24-methylenecholesterol) ($28\Delta^{5,24}$) (Volkman, 1986).

Hydrocarbons are also used as biomarker compounds to differentiate organic sources (Yunker et al., 1994, 1995). For example, the presence of C27, C29, and C31 n-alkanes indicates the land-plant wax sources (Eglinton and Hamilton, 1967). By contrast, algal contributions are indicated by the presence of C17 (Blumer et al., 1971; Robinson et al., 1987).

In the present study, molecular-level source-specific biomarkers such as fatty acids, sterols, and n-alkanes, in association with geochemical and biological indicators in river water collected from Pearl River basin were analyzed (1) to decipher the autochthonous and allochthonous OC sources; (2) to elucidate the relationship between aquatic photosynthesis and DIC concentrations; and (3) to illustrate the environmental factors that can control their organic carbon compositions.

2. Materials and methods

2.1. Study area

The Pearl River basin is the third longest (2214 km) and second largest (in terms of streamflow rate) river in South China. It has a drainage area of 4.42×10^5 km^2, which is an economically highly developed region with crucial position in the social-economic in South China (23°41′–29°15′N; 97°39′–117°18′E). The basin is located in the tropical and sub-tropical climate zones, with an annual average temperature of about 22 °C and an annual precipitation of about 1500 mm. The Pearl River basin is an extensive river system and consists of three major tributaries: Xijiang, Beijiang, and Dongjiang. Xijiang is the largest tributary that comprises the Nanpanjiang, Hongshuihe, Qianjiang, and Xijiang, and its main recharge sources are from Beipanjiang, Liujiang, Yujiang, and Guijiang (Fig. 1). Xijiang has a drainage area of 3.53×10^5 km^2, accounting for 77.8% of the total Pearl River basin drainage area, and its total length is 2075 km. Beijiang is the second largest tributary of the Pearl River with a length of 468 km and drainage area of 0.47×10^5 km^2. Dongjiang is approximately 520 km long with drainage area of 0.27×10^5 km^2, accounting for 6.6% of the total area of the Pearl River basin. The Pearl River is a typical carbonate rock area, which covers 1.58×10^5 km^2 and accounts for 35% of the total basin (Zhang et al., 2015). Xijiang basin is dominated by limestone and its upstream is the world famous karstic limestone area in south China. While the Dongjiang basin is mainly composed of granite and characterized as a silicate area. Rock types of Beijiang basin include limestone, dolomite and quaternary deposits.

2.2. Sample collection

Water samples were collected at 10 cm below the water surface during January to February 2015 when the basin was in the dry season. The sampling sites were set along the Pearl River, including its several main distributaries (Beipanjiang, Nanpanjiang, Hongshuihe, Xijiang, Liujiang, Guijiang, Beijiang, and Dongjiang) (Table 1). The sites were grouped according to the location of distributaries to represent different lithological, climatic and hydrological impacts. At each site, 500 mL of water were collected into the brown bottle. HCl was added to the samples to lower the pH to below 2. The samples were stored for GC–MS analysis. The bulk water chemical analysis was immediately performed by the WTW (Wissenschaftlich–Technische–Werkstaetten) Technology Multi-Line 350i to detect in situ water temperature (T), pH, dissolved oxygen (DO), and electrical conductivity (EC). The meters were calibrated prior to deployment using pH (4, 7, and 10), EC (1412 s/cm), and DO (0% and 100%) standards. The resolutions of pH, T, DO, and EC were 0.01, 0.01 °C, 0.01 mg/L and 1 μs/cm, respectively. Phytoplankton indicators were also analyzed in addition to geochemical and lipid indices. Chlorophyll a (Chl *a*) and biomass samples were collected and stored by adding 1% $MgCO_3$ and Lugols solution, respectively.

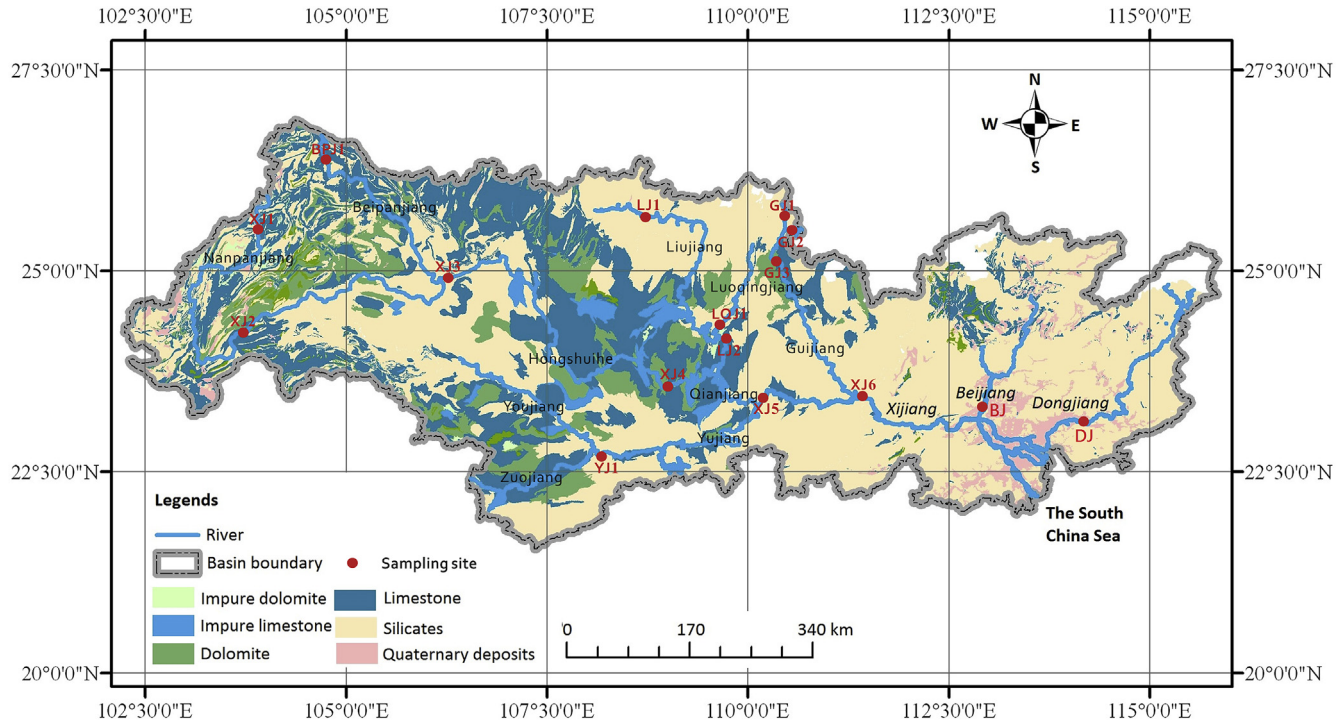

Fig. 1. Geology of the Pearl River and sampling sites.

Table 1
Information of sampling sites in the Pearl River.

Site	Location	Tributary description	TSS[a] (mg/L)	T[a] (°C)	Precipitation[a] (mm/a)
XJ1	25°36′18″N; 103°49′33″E	Upstream of Nanpanjiang	1290	18.6	1000.0
XJ2	24°01′13″N; 103°36′20″E	Midstream of Nanpanjiang	680	20.2	963.7
BPJ1	26°29′59″N; 103°44′07″E	Upstream of Beipanjiang	2610	18.7	1127.6
XJ3	24°57′47″N; 106°08′55″E	Junction of Nanpanjiang and Beipanjiang	170	19.1	921.1
XJ4	23°44′04″N; 109°13′43″E	Downstream of Hongshuihe	628	20.8	1499.8
YJ1	22°48′38″N; 108°18′46″E	Junction of Zuojiang and Youjiang	241	21.6	1304.2
LQJ1	24°24′09″N; 109°36′25″E	Downstream of Luoqingjiang	132	20.0	1257.7
LJ1	25°13′07″N; 109°23′47″E	Upstream of Liujiang	143	19.0	1493.0
LJ2	24°14′36″N; 109°43′13″E	Junction of Liujiang and Luoqingjiang	132	21.6	1304.2
XJ5	23°27′50″N; 110°09′39″E	Junction of Qianjiang and Yujiang	350	21.4	1726.7
GJ1	25°31′17″N; 110°11′41″E	Upstream of Guijiang	67	18.0	2052.0
GJ2	25°06′19″N; 110°24′55″E	Upstream of Guijiang	92	18.7	1926.0
GJ3	25°16′40″N; 110°18′14″E	Midstream of Guijiang	105	19.0	1894.4
XJ6	23°28′40″N; 111°17′11″E	Downstream of Xijiang	311	21.1	1503.6
BJ	23°41′21″N; 113°03′26″E	Downstream of Beijiang	129	20.7	1900.1
DJ	23°09′28″N; 114°16′12″E	Downstream of Dongjiang	107	22.1	1821.2

[a] Annual mean value, reference from Pearl River Water Resource Commission of the Ministry of Water Resources (http://www.pearlwater.gov.cn).

2.3. Bulk chemical analysis

The concentrations of HCO_3^- and Ca^{2+} represent the intensity of rock weathering and chemical processes in the aquatic system. The in situ measurement kit by Merck (German) was used to precisely measure these two parameters and the resolutions were 0.1 mmol/L (HCO_3^-) and 4 mg/L (Ca^{2+}), respectively (Liu et al., 2007). Anion concentrations of F^-, Cl^-, NO_3^-, and SO_4^{2-} were measured in the laboratory using the ion chromatograph ICS–90 Dionex. The cations were analyzed through ICP–OES Vista MPX (Varian, USA). Ion concentrations were used to calculate the CO_2 partial pressure (pCO_2) and calcite saturation index (SIc) from a geochemical model with pH, temperature, and seven major ions concentrations using the WATSPECT program (Wigley, 1977).

Chl *a* was concentrated from water sample through filtration with vacuum filtration and then extracted using an acetone 90% solution. Concentrations of Chl *a* were determined through UV spectrometer according to standard methods established by the Ministry of Environmental Protection of China (MEP, 2002). Additionally, the biomass amount of each water sample was counted through blood counting chamber. The TSS concentrations were collected by filtering the water samples immediately with GF/F glass fiber filters (47 mm diameter; Whatman International) that were pre-combusted at 450 °C for at least 5 h. The filters loaded with SPM were then stored in plastic bags at −20 °C and re-weighed in the laboratory to obtain TSS concentrations. OD680, and turbidity of water samples were determined through UV–spectrophotometer according to the standard methods (MEP, 2002).

2.4. Lipid biomarker analysis

Total organic compounds in water samples were extracted in a

solution of dichloromethane: methanol (MeOH) using a liquid–liquid extractor. Extracts were divided into two phases, and the lower organic phase was collected. Then, the samples were re-extracted by hexane, and the combined organic phase sat over anhydrous Na_2SO_4 overnight to reduce traces of water. The samples were concentrated to 1 mL using rote-evaporation. A portion of the extract was saponified using 1 M KOH in aqueous MeOH. Neutral and acidic lipids were extracted into hexane from the saponified sample. Fatty acids were converted to methyl esters using BF3–⊖ MeOH. Both fatty acids and neutral lipids were separated from other lipid classes by silica gel chromatography. Sterols were derivatized to trimethylsilyl (TMS) ethers using BSTFA and acetonitrile and heating at 70 °C for 30 min (Waterson and Canuel, 2008).

Fatty acid (as methyl esters), sterols (as TMS ethers), and n-alkanes were analyzed using gas chromatography (GC) (Agilent 7890A) with FID (flame ionization detection) using a 30 m × 0.32 mm × 0.25 μm DB5 column. Individual compounds were identified by comparing the retention time to the results obtained from external standards (fatty acid methyl esters mixture standard, sterols mixture standard and C8–C40 n-alkanes standard, Sigma–Aldrich Company). Compounds were quantified using total ion current (TIC) peak area and converted to compound mass using calibration curves of external standards. The GC conditions were as follows: For fatty acids, temperature was programmed from 60 °C to 150 °C at 40 °C/min. Then, the temperature was increased to 240 °C (held for 15 min) at 3 °C/min; For sterols, temperature was raised from 80 °C (held for 1 min) to 200 °C at 25 °C/min, and then at 3 °C/min to 250 °C, followed by 1.8 °C/min to 300 °C (held for 2 min); For n-Alkanes, temperature was raised from 70 °C (held for 1 min) to 140 °C at 10 °C/min, and then at 3 °C/min to 310 °C (held for 15 min) (Mortillaro et al., 2011).

2.5. Data analysis

Principal Component Analysis (PCA) is a multivariate statistical technique that is used to analyze environmental variations (Faucon et al., 2011; Grenouillet et al., 2011) based on the investigated species and community characteristics, sometimes in combination with canonical correspondence analysis (CCA) (Marmion et al., 2009; Mezger and Pfeiffer, 2011). PCA has been applied in ecological environment research. This analytical method assists in evaluating aquatic habitat suitability, as well as in interpreting seasonal and spatial variation and change in ecosystem organization, in aquatic system studies (Ahmadi-Nedushan et al., 2006; Blanck et al., 2007). PCA and CCA were conducted using lipid biomarkers, phytoplankton, and geochemical characteristics from 16 sites to analyze the mutual influences of the environmental geochemical parameters and their relation with the carbon sink.

3. Results

3.1. Geochemical compositions of riverine water

The results are shown in Fig. 2. HCO_3^- concentrations in the Pearl River exhibited large spatial difference. The highest value was 4.6 mmol/L at XJ1 site located in the upper Nanpanjiang, with a primarily carbonate bed rock (Fig. 1). The lowest value was 0.4 mmol/L at GJ1 site (upper Guijiang), which was in a silicate area (Fig. 1). Remarkably decreased HCO_3^- concentration was observed from the mountainous topography in Guizhou and Yunnan provinces to the estuary area of Guangzhou province. Average Ca^{2+} concentration was 46.1 mg/L, ranging from 88.0 mg/L (XJ1) to 10.0 mg/L (GJ1), which was consistent with the DIC concentration. Thus, HCO_3^- concentration in the Pearl River was primarily controlled by dissolution of carbonate minerals.

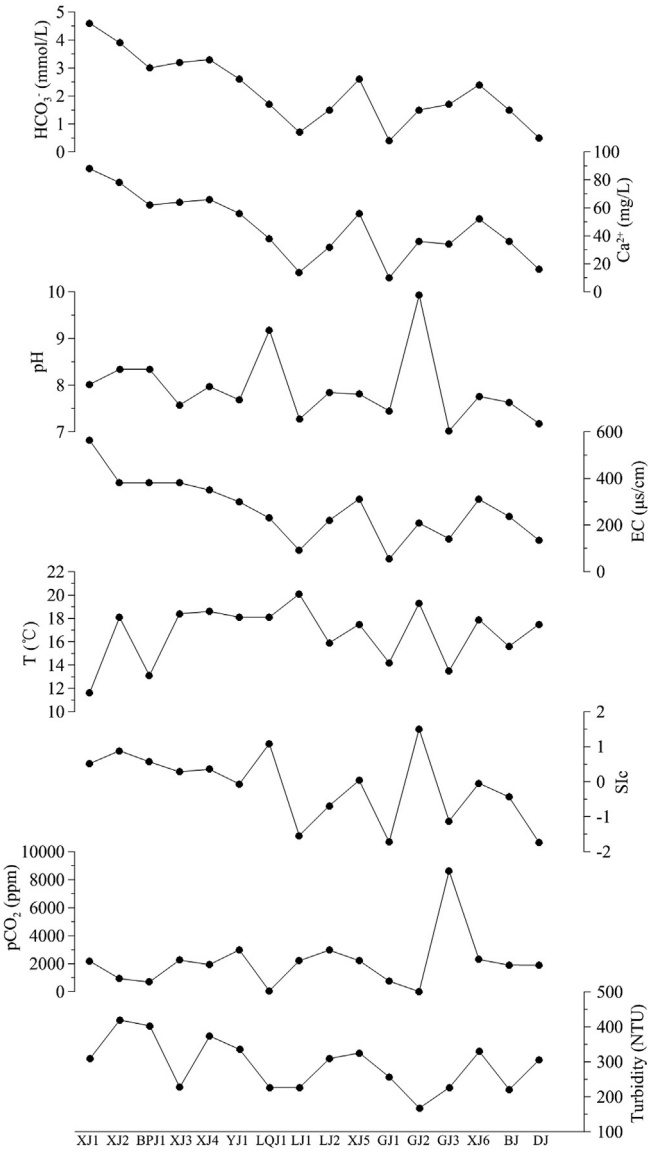

Fig. 2. Geochemical characteristics of the Pearl River water at different sites. EC: specific electrical conductivity (μs/cm); T: water temperature (°C); SIc: calculated calcite saturation index; pCO_2: calculated CO_2 partial pressure (ppm).

Calculated pCO_2 in the Pearl River displayed obvious spatial differences, ranging from 4.1 ppm to 8629.8 ppm (average 2118.2 ppm). SIc ranged from −2.14 to 1.51 (average, −0.13). Significant positive correlation was found between EC values and HCO_3^- concentrations in the Pearl River ($R^2 = 0.92$, $P < 0.0001$), demonstrating that the primary mechanism for the chemical composition of river water was rock weathering. Overall, the monitoring sites could be divided into three groups based on the HCO_3^- concentrations: high HCO_3^- group (XJ1, XJ2, XJ3, XJ4, and BPJ1), moderate HCO_3^- group (YJ1, LJ2, XJ5, and XJ6) and low HCO_3^- group (LJ1, LQJ1, GJ1, GJ2, GJ3, BJ, and DJ). This classification was further confirmed by the phytoplankton indices described in section 3.2.

3.2. Lipid biomarker compositions of river water

3.2.1. Fatty acids

The total fatty acid (TFA) concentrations were between 11.4 μg/L and 311.8 μg/L, with average of 75.9 μg/L. The highest and lowest

values were obtained at XJ2 and GJ1, respectively. The TFA concentrations varied with those of HCO_3^-, from 129.7 μg/L (ranging from 62.7 μg/L to 311.8 μg/L) at sites with high HCO_3^- concentrations to 35.1 μg/L (ranging from 11.4 μg/L to 56.1 μg/L) at sites with low HCO_3^- concentrations. Fatty acids were composed of saturated and unsaturated fatty acids. Saturated fatty acids were divided into straight saturated fatty acids (SSFA) and branched saturated fatty acids (BSFA). SSFA, the most abundant class with dominated by short-chain saturated fatty acids over long-chain saturated fatty acids, accounted for 63.8% of the TFAs. Unsaturated fatty acids included MUFA and PUFA. Mean percentage of MUFA was 13.2%, whereas those of PUFA and BSFA were 13.1% and 9.9% of the TFA, respectively (Table 2). Individual compounds of fatty acids also showed difference among sites. C16:0 (Palmitic acid) was the most abundant compound, which accounted for an average of 20.0% of the TFA. The MUFA usually represent the activity of diatom growth in aquatic systems and have been used to evaluate the autochthonous production capacity (Dunstan et al., 1993a). C16:1ω (Palmitoleic acid) was the major MUFA and considered as indicator of autochthonous production. This fatty acid was observed in all water samples of the Pearl River. Water sample at XJ3 contained the most abundant C16:1ω (23.5 μg/L), whereas DJ had the lowest value (3.6 μg/L). The presence of C16:1ω indicated that the photosynthesis of phytoplankton was intense in the Pearl River (Viso and Marty, 1993). By contrast, C18:2ω (Linoleic acid) indicated carbon source derived from terrestrial plant via fluvial erosion. The concentration of C18:2ω ranged from 0.2 μg/L to 17.9 μg/L.

3.2.2. Sterols

Concentrations of total sterol ranged from 1.1 μg/L to 3.6 μg/L, with an average value of 2.4 μg/L. The most abundant sterol at all sites was 24α-methylcholesta-5,22*E*-dien-3β-ol ($28\Delta^{5,22}$), which varied from 0.3 μg/L to 1.7 μg/L. Highest concentration of $28\Delta^{5,22}$ was detected in the upstream major tributaries (XJ3) which was covered mainly by carbonate rocks (Fig. 1). By contrast, the lowest concentration was observed at DJ, which was dominated by silicate rock (Fig. 1). Cholest-5-en-3β-ol ($27\Delta^5$) had the same distribution pattern with $28\Delta^{5,22}$, and its average value was 0.8 μg/L 24-methylcholest-5-en-3β-ol ($28\Delta^5$) and 24-ethylcholesta-5,22*E*-dien-3β-ol ($29\Delta^{5,22}$) were particular proxies for terrestrial plants sources (Li et al., 1995). Their concentrations in the Pearl River ranged from 0.2 μg/L to 0.8 μg/L (average, 0.4 μg/L) and 0.1 μg/L to 0.4 μg/L (average, 0.3 μg/L), respectively. Concentrations of $28\Delta^5$ and $29\Delta^{5,22}$ were found to be enriched at downstream sites where various materials were drained, contrary to $28\Delta^{5,22}$ and $27\Delta^5$.

3.2.3. n-Alkanes

n-Alkane concentrations ranged from 601.3 μg/L to 2316.5 μg/L (average, 1311.8 μg/L) and contained compounds from C12 to C34, with C17 as the most abundant compound (35.6 μg/L to 311.2 μg/L; average, 149.3 μg/L). CPI_{HC}, which was defined using the equation of Bianchi (2007), was 2.99 on average and ranged from 1.18 to 4.99 (Table 2). CPI_{HC} was highest in the upstream tributaries with high flow rates. TAR_{HC} represents the terrestrial-to-aquatic ratio, which was developed as a proxy for assessing the relative contributions of autochthonous and allochthonous hydrocarbons in aquatic environments (Meyers, 1997). Calculated TAR_{HC} in the Pearl River water ranged from 0.26 to 0.63 with average value of 0.52.

3.3. Phytoplankton features of river waters

DIC (mainly HCO_3^-) is utilized to form OC and release O_2 during the photosynthesis in the aquatic ecosystem (ref. Eq. (1)). Phytoplanktons, especially algae, are the typical products of these coupled interactions and serve as a potential carbon sink. Thus, elucidating the features of phytoplankton and their relation with DIC distribution is of interest.

Chl *a* is a major parameter to explain the primary products in the aquatic system because it participates in photosynthesis. The average concentration of Chl *a* in the different samples from the Pearl River was 6.3 mg/m^3, which was higher than that in Yangtze River, showing the intense photosynthesis process (Zheng et al., 2013). However, the high concentration of Chl *a* may not have been fully caused by in situ aquatic photosynthesis but may also be derived from terrestrial flushing materials. For example, Chl *a* concentrations at XJ2 and XJ3 were 9.9 and 9.0 mg/m^3 (Fig. 3), respectively. However, the phytoplankton biomass showed large differences (2.2×10^6 cell/L and 3.5×10^6 cell/L, respectively, Fig. 3).

Table 2
Detected lipid biomarkers and calculated proxies in the Pearl River.

Site	Fatty acids				Sterols			n-Alkanes		
	SSFA (%)	BSFA (%)	MUFA (%)	PUFA (%)	$28\Delta^{5,22}$ (μg/L)	$29\Delta^5$ (μg/L)	$27\Delta^5/29\Delta^{5,22}+29\Delta^5$	TAR_{HC}	CPI_{HC}	C17 (μg/L)
XJ1	72.0	2.2	19.7	6.1	1.2	0.2	4.79	0.38	1.56	296.3
XJ2	66.5	8.3	17.5	7.7	1.5	0.4	4.32	0.61	2.09	255.3
BPJ1	60.3	8.4	16.5	14.7	0.9	0.2	3.53	0.55	2.12	266.3
XJ3	61.2	4.1	23.8	10.8	1.7	0.1	7.29	0.26	1.18	311.2
XJ4	65.4	3.8	19.2	11.6	0.9	0.2	3.90	0.47	2.92	216.3
YJ1	53.5	10.8	13.7	22.1	1.5	0.2	1.89	0.59	3.43	243.2
LQJ1	62.9	12.7	6.6	17.8	1.1	0.3	2.79	0.61	3.79	163.2
LJ1	55.0	21.7	10.0	13.4	0.4	0.2	1.45	0.48	2.28	35.6
LJ2	77.1	3.7	14.8	4.4	0.4	0.2	0.81	0.52	4.99	35.6
XJ5	62.2	4.8	12.8	20.1	0.6	0.3	2.02	0.52	2.88	189.0
GJ1	62.7	17.2	8.7	11.4	0.4	0.2	0.67	0.49	3.32	47.7
GJ2	63.3	16.5	7.2	13.0	0.7	0.2	1.59	0.46	3.52	69.9
GJ3	63.2	16.1	4.5	16.3	0.7	0.2	2.00	0.43	3.71	57.0
XJ6	58.6	12.2	15.6	13.6	1.3	0.3	1.99	0.51	2.33	68.0
BJ	72.5	6.4	11.7	9.5	0.9	0.4	0.89	0.68	4.71	88.8
DJ	63.9	10.1	9.9	16.0	0.3	0.4	1.11	0.72	3.16	45.2
mean	63.8	9.9	13.3	13.0	0.9	0.3	2.57	0.52	2.99	149.3

SSFA (straight saturated fatty acids), BSFA (branched saturated fatty acids), MUFA (monounsaturated fatty acids), and PUFA (polyunsaturated fatty acids) were calculated by their concentration normalized to total fatty acids, respectively; $28\Delta^{5,22}$: 24α-methylcholesta-5,22*E*-dien-3β-ol; $29\Delta^5$: 24-ethylcholest-5-en-3β-ol; $27\Delta^5$: cholest-5-en-3β-ol; $29\Delta^{5,22}$: 24-ethylcholesta-5,22*E*-dien-3β-ol; TAR_{HC} = (C27 + C29 + C31)/(C15 + C17 + C19). $TAR_{HC} > 1$ indicates vascular plants derived source, while $TAR_{HC} < 1$ reflects a dominance of hydrocarbons of aquatic origin (Meyers, 1997); The CPI_{HC} proxy (CPIHC = 0.5[(C25 + C27 + C29 + C31 + C33/C24 + C26 + C28 + C30 + C32) + (C25 + C27 + C29 + C31 + C33/C26 + C28 + C30 + C32 + C34)]) shows whether hydrocarbon biomarkers reflect contributions from terrestrial plants (high CPI_{HC}) or aquatic sources (low CPI_{HC}) (Bianchi, 2007); C17: Heptadecane.

This Chl *a* concentrations at XJ2 may have been caused by the terrestrial plants, which also contained Chl *a*, flowed into the river by fluvial erosion. This process resulted in the relatively high Chl *a* concentration, but low phytoplankton biomass.

Photosynthesis in aquatic system can result in high accumulation of biomass in a short period of time and over a relatively large area. The average phytoplankton biomass from 16 sites was 2.0×10^6 cell/L. The highest phytoplankton biomass (3.5×10^6 cell/L) was detected at XJ3 (Fig. 3) that was characterized by high DIC, low water flow, and low TSS concentration, which provided sufficient carbon source and suitable environment for photosynthesis. By contrast, DJ was recharged with low DIC and high water flow, and the biomass was low at 1.0×10^6 cell/L (Fig. 3).

OD680, which is another parameter in phytoplankton research, was used to trace the growth state of aquatic phytoplankton. The OD680 values were consistent with biomass (Fig. 3), which showed that phytoplankton at upstream sites with high DIC concentrations grew more rapidly. However, downstream sites with low DIC concentrations also offered suitable growth environment for phytoplankton but the OD680 at DJ was 2.88 times lower than that at XJ3 (Fig. 3).

4. Discussion

The H_2O–carbonate–CO_2–aquatic phototroph interaction model (Eq. (1)) was established to determine whether carbonate weathering-derived DIC could be converted into stable carbon sink and finally offer a new direction for finding the missing carbon sink (Liu et al., 2010, 2011; Liu and Wolfgang, 2015). Photosynthetic uptake of DIC by aquatic phototroph was the fundamental part of this model, with emphasis on the introduction of autochthonous OC in the calculation of carbonate weathering-related carbon sink. We first traced the OC sources using lipid biomarkers and discussed their relation with DIC concentrations. PCA analysis was then conducted to explore the regional diversity of chemical compositions, and finally, influences of environmental factors were investigated.

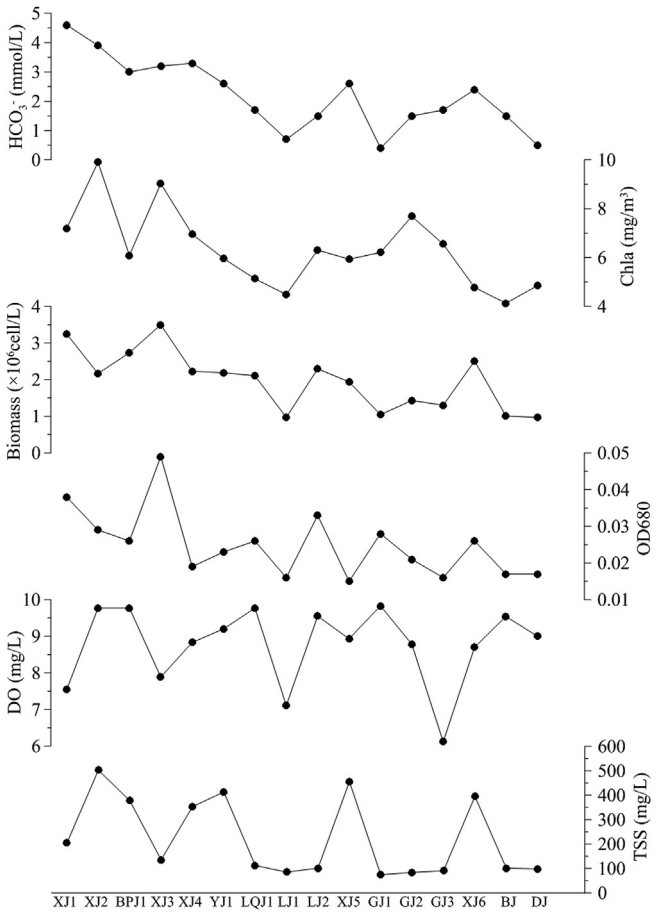

Fig. 3. Phytoplankton characteristics of Pearl River water at different sites. HCO_3^-: the concentration of HCO_3^- in water sample (mmol/L); Chl *a*: the concentration of Chlorophyll a in water sample (mg/m^3); Biomass: the concentration of phytoplankton in water sample ($\times 10^6$ cell/L); OD680: the optical density at 680 nm; DO: the concentration of dissolved oxygen in water sample (mg/L); TSS: the concentration of total suspended solid in water sample (mg/L).

4.1. OC sources and DIC fertilization effect on aquatic photosynthesis

Organic carbon sourcing in the Pearl River is complex in terms of amount, type, and distribution subject to processes including rock weathering, photosynthetic activity, and fluvial erosion. Source-specific-based lipid biomarker is extensively used to distinguish between autochthonous and allochthonous OC sources. The ratio of autochthonous and allochthonous OCs represents the in situ productivity of aquatic system over allochthonous input. Results showed that autochthonous organic source in the Pearl River was the dominant input with ratio larger than 65% on average (Fig. 4). This value was comparable with the calculation conducted by Waterson and Canuel (2008), which showed that the contribution of autochthonous OC was larger than 62% in the Mississippi River. The autochthonous percentage showed a positive correlation with the biomass of phytoplankton ($R^2 = 0.7710$, $P < 0.0001$), which indicated that in situ primary productivity was the major contributor to the autochthonous OC.

Biomass, autochthonous percentage, and C16:1ω/C18:2ω were all positively correlated with HCO_3^- concentrations in the Pearl River (Fig. 5). This finding indicates the DIC fertilization effect on the in-river primary production.

DIC apparently significantly promoted the growth of phytoplankton as shown by the positive correlation between biomass and HCO_3^- ($R^2 = 0.6685$). Phytoplankton gained more carbon supplement and then bloomed rapidly, especially at XJ1 and XJ3, with high HCO_3^- concentrations. Meanwhile, biomarkers derived from phytoplankton were produced and their concentrations can also indicate the photosynthesis process. For example, C16:1ω/C18:2ω was positively correlated with HCO_3^- ($R^2 = 0.6479$), indicating that high HCO_3^- concentration in the aquatic system caused the high autochthonous OC percentage.

4.2. Autochthonous and allochthonous sources of OC and their geochemical indications

In order to understand the potential inherent connection between numerous biomarkers and a large number of samples, PCA and CCA were conducted to provide a robust classification of biomarkers according to their primary sources and illustrate the influences of environmental features (Fig. 6). As shown in Fig. 6, factor 1 explained 65.8% of the variance in the data set, apparently to separate the data based on the relative abundance of autochthonous versus allochthonous sources of organic matter and their relative proxies. Positive factor 1 included lipid biomarkers, namely, C16:1ω/C18:2ω, MUFA(%), $28\Delta^{5,22}$, $27\Delta^5$, $27\Delta^5/29\Delta^{5,22} + 29\Delta^5$, and C17, and phytoplankton proxies, namely, Chl *a*, OD680, and biomass. These parameters were positively correlated and showed that the sources were characterized by autochthonous (also at the same direction). On the contrary, the negative factor 1 then reflected the allochthonous source shown by the indices BSFA (%),

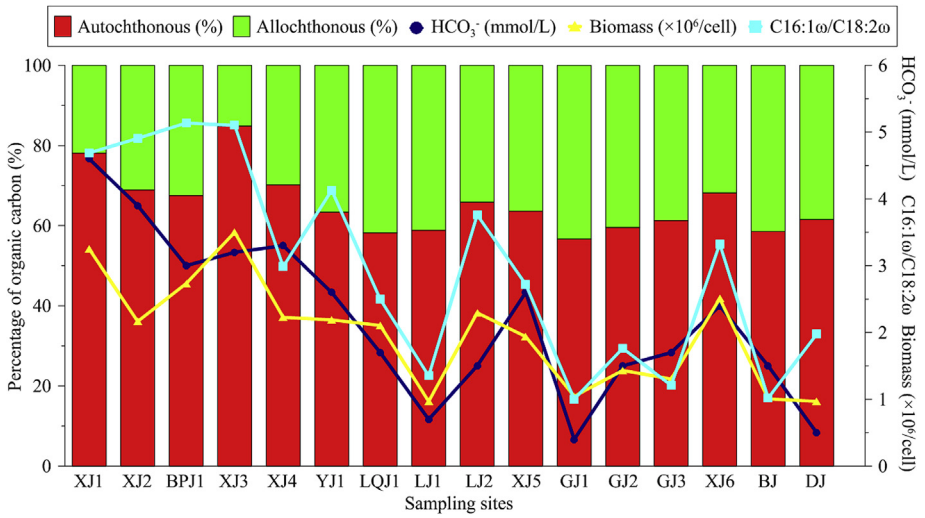

Fig. 4. Spatial distributions of percentages of autochthonous and allochthonous OC and the hydrochemical (HCO_3^-) and biological (C16:1ω/C18:2ω and biomass) indices. C16:1ω/C18:2ω ratio was used to evaluate the relative contribution of algal vs. terrestrial plants; Autochthonous (%) and Allochthonous (%) are percentages of even and odd numbered saturated short chain fatty acids (C12–C18) and even and odd numbered saturated long chain fatty acids (C22–C30) normalized to total saturated fatty acids, respectively (Waterson and Canuel, 2008).

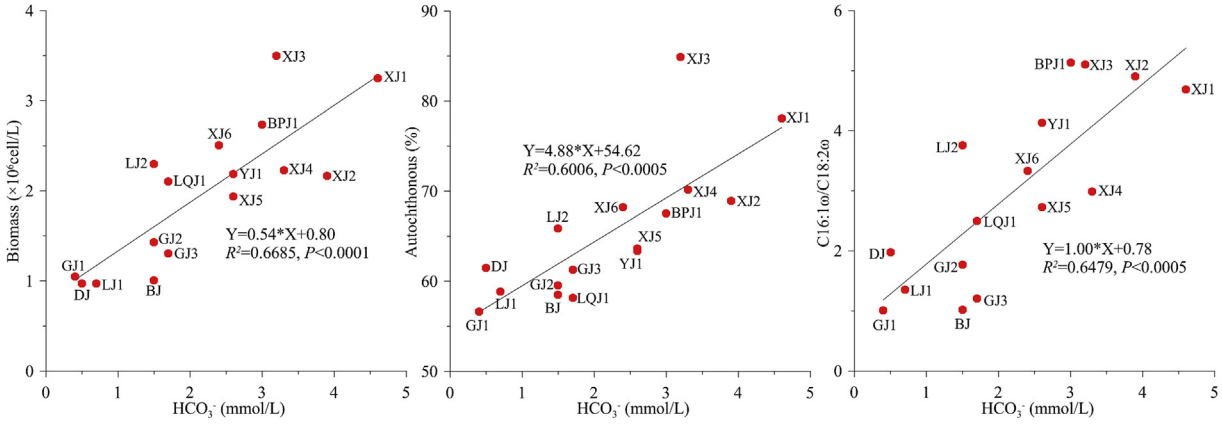

Fig. 5. Relationship between biomass, autochthonous (%), or lipid biomarker (C16:1ω/C18:2ω) indices and HCO_3^-.

$28\Delta^5$, $29\Delta^{5,22}$, TAR_{HC}, and CPI_{HC}. TAR_{HC} ratios were below 1 throughout the Pearl River, indicating that the dominant OC source was aquatic autochthonous. Higher TAR_{HC} ratios were found at BJ and DJ (TAR_{HC} = 0.68 and 0.72, respectively), where high flow rates were detected during sample collection. These sites demonstrated almost equal contributions from both allochthonous and autochthonous sources. Characteristics, such as TSS, Chl *a*, and SSFA (%), plotted intermediate between the autochthonous and allochthonous indices, suggesting a mixed source.

Score plots were used to examine the relationships between the factors and each sample. Although XJ2 had the highest TSS concentration, DIC was also high, which indicated that fluvial erosion offered terrestrial organic source, and DIC was uptaken to synthesize autochthonous sources. The other constrains also proved this pattern. For example, $28\Delta^{5,22}$ and $29\Delta^{5,22}$ were high at this site, indicating the mixed input of autochthonous and allochthonous sources. Samples collected from high DIC areas had the most positive factor 1 scores, which demonstrated that OC at these sites could be attributed to autochthonous source. XJ3, for example, was upstream of the Pearl River in Guizhou province, where karst process was quite intense and considered as the primary region of carbonate weathering in China. XJ3 was a typical site characterized by high DIC concentration and EC, which offered continuous carbon source for photosynthetic activity and increased the amount of autochthonous source. In addition, low flow rate and additional sunshine penetration in the river water enhanced the primary production. Similar sites, such as XJ1, XJ4, and BPJ1 indicate the autochthonous input source.

By contrast, water samples with low DIC had negative scores of factor 1 (Fig. 6). Sites with negative factor 1 scores were LJ1, LQJ1, GJ1, GJ2, GJ3, BJ and DJ. Their lipid compositions were characterized by higher PUFA(%). Additionally, $28\Delta^5$ and $29\Delta^{5,22}$ were biomarkers originating from terrestrial plants and located at the negative factor 1, which were positively correlated with BSFA(%) and mainly formed by fluvial erosion.

The remaining sites were plotted at an intermediate position, with negative scores on factor 1, especially at sites located downstream that received multiple materials coming along with the river flow.

The TAR_{HC} ratio, autochthonous (%), biomass, etc. under the three DIC patterns were compared in Fig. 7. Three patterns based on the DIC concentration had obvious distinction, indicating that DIC in riverine system is the driving force for chemical and aquatic photosynthetic activities.

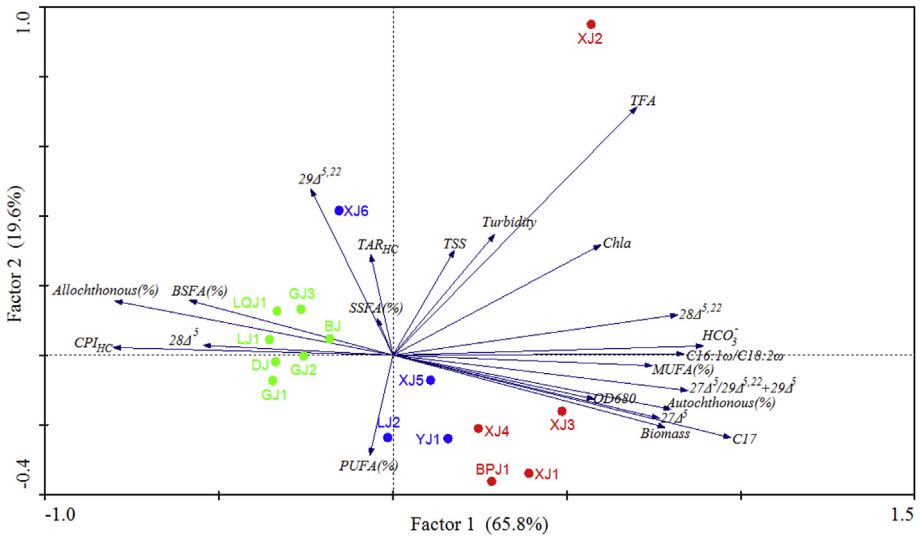

Fig. 6. Results from the PCA and CCA analysis. Factor 1 explained 65.8% of the variance and distinguished between autochthonous and allochthonous organic sources. Biomarkers representing autochthonous organic sources (e. g., C16:1ω/C18:2ω, MUFA(%), $28\Delta^{5,22}$, $27\Delta^5$, $27\Delta^5/29\Delta^{5,22} + 29\Delta^5$, and C17) had positive loadings while allochthonous organic sources (e. g., BSFA(%), $28\Delta^5$, $29\Delta^{5,22}$, TAR_{HC}, and CPI_{HC}) had negative values. Factor 2 explained 19.6% of the variance and indicated the influence of fluvial erosion by using the TSS and turbidity. Sampling sites XJ1, XJ2, XJ3, XJ4, and BPJ1 belong to high HCO_3^- group, YJ1, LJ2, XJ5, and XJ6 belong to moderate HCO_3^- group, and LJ1, LQJ1, GJ1, GJ2, GJ3, BJ, and DJ belong to low HCO_3^- group.

4.3. Impacts of TSS on phytoplankton photosynthesis

TSS was at the moderate position of factor 1 axis (Fig. 6) with high score, indicating its significant influence on the supplement of OC in riverine system, particularly at regions characterized by intense fluvial erosion. The influence of TSS on in situ primary production in the Pearl River could be divided into two patterns, namely, inhibiting and promoting patterns (Fig. 8). The inhibiting pattern was caused by the following: 1) TSS reflected the intensity of fluvial erosion that delivered the terrestrial OC into river and increased the amount of allochthonous source; and 2) high TSS concentration (TSS > 150 mg/L) on the water surface blocked the light and then reduced the production of phytoplankton. Thus, light limitation was a major constrain on phytoplankton production. The two processes mixed together and finally increased the allochthonous proportion. For example, YJ1 had a very high TSS concentration, but its autochthonous (%) was as low as 63.34%, which proved the negative TSS effect. However, even with high TSS concentration, the in situ photosynthesis of phytoplankton could also produce autochthonous OC. XJ2 was the typical site for such conditions, in which autochthonous (%) was as high as 68.93%, which also showed the dominant role of in situ primary produced organic carbon.

Interestingly, low TSS concentration (TSS < 150 mg/L) seems to promote the photosynthesis activity according to the positive correlation between autochthonous percentage or phytoplankton biomass and TSS (Fig. 8). This phenomenon occurred at XJ3, LQJ1, LJ1, LJ2, GJ1, GJ2, GJ3, BJ and DJ. A certain amount of TSS could have adsorbed the phytoplankton, which provided the nutrients and growing room, hence increasing the phytoplankton biomass. This process was consistent with previous results that bacteria were transported and attached onto suspended particles (Mahler et al., 2000). Thus, TSS impacts on the phytoplankton photosynthesis should be assessed on the basis of fluvial erosion and photosynthesis activity.

5. Conclusion

Measurements of biomarker, phytoplankton, and geochemical features of surface river water demonstrated spatial variation in the sources of inorganic and organic carbon within the Pearl River. DIC sources were mainly controlled by lithological characters and river-flow dynamics because DIC in riverine system primarily originated from soil CO_2 and atmospheric CO_2. Specifically, DIC distributions in 16 sites in the Pearl River had three patterns, namely, high (XJ1, XJ2, XJ3, XJ4, and BPJ1), low (LJ1, LQJ1, GJ1, GJ2, GJ3, BJ, and DJ), and moderate (YJ1, LJ2, XJ5, and XJ6) DIC areas. Quantitative organic source assignments of water samples were conducted using lipid biomarkers (fatty acids, sterols, and n-alkanes) and the percentage contributions of allochthonous and autochthonous sources were calculated to create a synopsis of the sources of organic material throughout the region. The following conclusions could be drawn:

Lipid biomarkers can be a useful tool in tracing organic sources. The calculated average autochthonous OC (based on fatty acids) was approximately 65% of the total OC, indicating intense in-river primary productivity in the Pearl River. SSFA, C16:0, C16:1ω, $28\Delta^{5,22}$, and C17 were positively correlated with phytoplankton proxies (biomass and OD680). Hence, these parameters are attributed to aquatic organic sources. By contrast, PUFA, $28\Delta^5$, and $29\Delta^{5,22}$ were derived predominantly from terrestrial contributions, which sensitively responded to fluvial erosion.

Autochthonous organic sources were positively correlated with DIC concentrations, which could be a DIC fertilization effect. This phenomenon is also shown by the growth of phytoplankton, which demonstrated a coupled process that consumed DIC source for their bloom and produced specific lipid organic sources.

TSS reflected the fluvial erosion that delivered the terrestrial OC into the river and increased the amount of allochthonous sources. High TSS (TSS > 150 mg/L) on the water surface blocked sunlight and then reduced the production of phytoplankton. However, in situ photosynthesis of phytoplankton could also produce autochthonous OC, even larger than the allochthonous source at sites with high DIC concentrations, even with higher TSS concentrations. Low TSS concentration (TSS < 150 mg/L) apparently promoted photosynthesis activity by offering nutrients and growth room. Therefore, DIC could be converted into OC, whose amount was even larger than the allochthonous source. These findings comprehensively elucidated the formation of autochthonous OC based on the coupling action of rock weathering and photosynthetic activity in

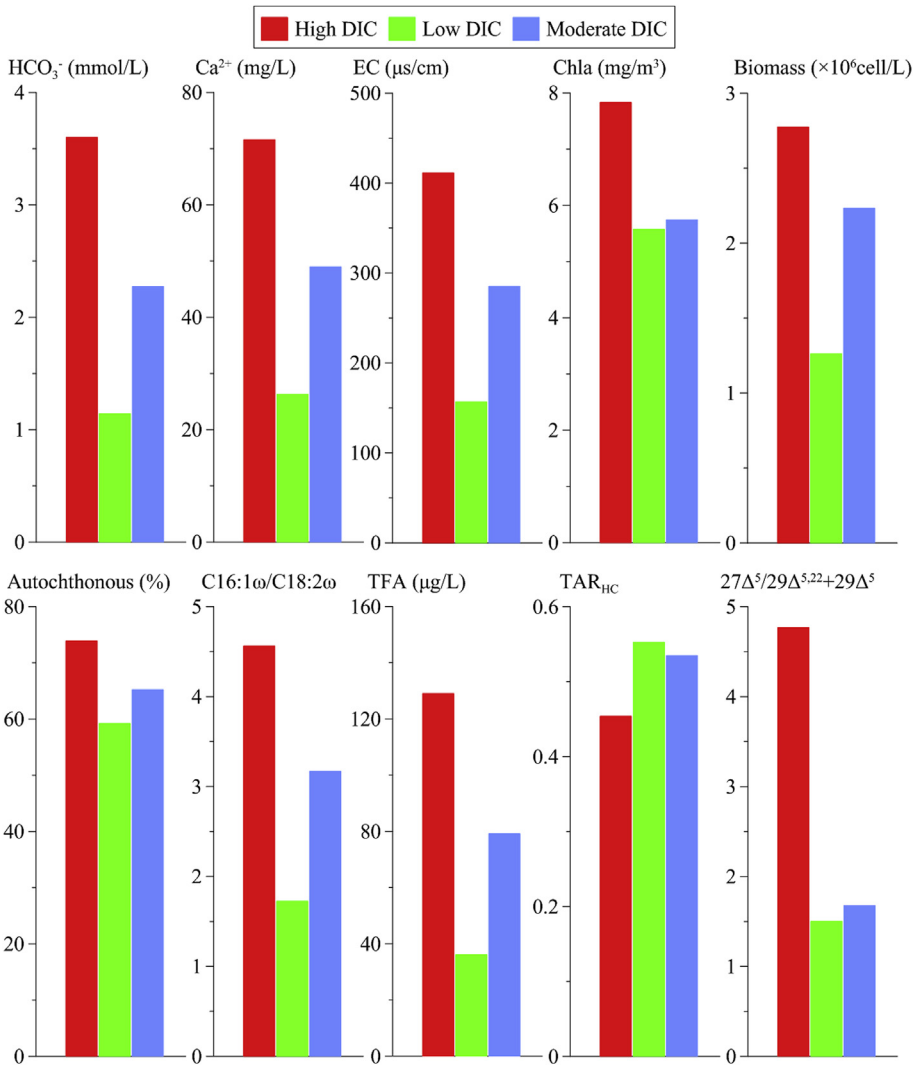

Fig. 7. Comparison of lipid biomarkers, phytoplankton, and geochemical proxies under the three DIC patterns. High DIC pattern represented sites with HCO_3^- concentration higher than 3.3 mmol/L; Low DIC pattern represented sites with HCO_3^- concentration lower than 1.7 mmol/L; Moderate DIC pattern represented sites with HCO_3^- concentration between the two extreme values.

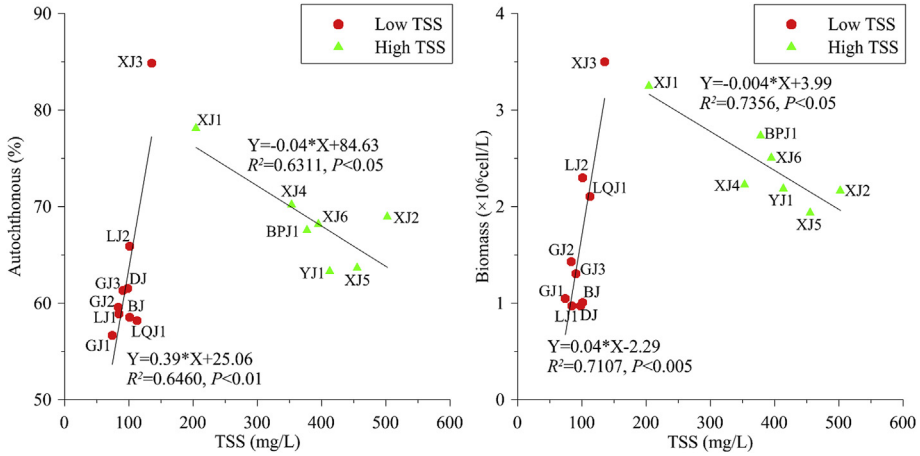

Fig. 8. Influence of TSS on the photosynthesis of phytoplankton. Low TSS represented concentration of TSS lower than 150 mg/L; High TSS represented concentration of TSS higher than 150 mg/L.

the riverine system, suggesting a potential direction for finding the missing carbon sink.

Acknowledgements

This work was supported by the National Basic Research Program of China (973 Program 2013CB956703), the National Natural Science Foundation of China (41430753) and the China Postdoctoral Science Foundation (Y5UN903000). We thank all our colleagues who provided help in the field investigation and lab analysis.

References

Ahmadi-Nedushan, B., St-Hilaire, A., Bérubé, M., Robichaud, É., Thiémonge, N., Bobée, B., 2006. A review of statistical methods for the evaluation of aquatic habitat suitability for instream flow assessment. River Res. Appl. 22, 503–523.
Bianchi, T.S., 2007. Biogeochemistry of Estuaries. Oxford University Press, New York.
Bianchi, T.S., Canuel, E.A., 2011. Chemical Biomarkers in Aquatic Ecosystems. Princeton University Press, Princeton and Oxford.
Blanck, A., Tedesco, P.A., Lamouroux, N., 2007. Relationships between life-history strategies of European freshwater fish species and their habitat preferences. Freshw. Biol. 52, 843–859.
Blumer, M., Guillard, R.R.L., Chase, T., 1971. Hydrocarbons of marine phytoplankton. Mar. Biol. 8, 183–189.
Burns, K.A., Hernes, P.J., Brinkman, D., Poulsen, A., Benner, R., 2008. Dispersion and cycling of organic matter from the Sepik River outflow to the Papua New Guinea coast as determined from biomarkers. Org. Geochem. 39, 1747–1764.
Cloern, J.E., Canuel, E.A., Harris, D., 2002. Stable carbon and nitrogen isotope composition of aquatic and terrestrial plants of the San Francisco Bay estuarine system. Limnol. Oceanogr. 47, 713–729.
Cole, J.J., Prairie, Y.T., Caraco, N.F., McDowell, W.H., Tranvik, L.J., Stregl, R.G., Duarte, C.M., Kortelainen, P., Downing, J.A., Middelburg, J.J., Melack, J., 2007. Plumbing the global carbon cycle: integrating inland waters into the terrestrial carbon budget. Ecosystems 10, 172–185.
Conte, M.H., Eglinton, G., Madureira, L.A.S., 1995. Origin and fate of organic biomarker compounds in the water and sediments of the eastern North Atlantic. Philos. Trans. R. Soc. B Biol. Sci. 348, 169–178.
Dalsgaard, J., John, M.S., Kattner, G., Müller-Navarra, D., Hagen, W., 2003. Fatty acid trophic markers in the pelagic marine environment. Adv. Mar. Biol. 46, 225–340.
Dunstan, G.A., Volkman, J.K., Barrett, S.M., Garland, C.D., 1993a. Changes in the lipid composition and maximisation of the polyunsaturated fatty acid content of three microalgae grown in mass culture. J. Appl. Phycol. 5, 71–83.
Dunstan, G.A., Volkman, J.K., Barrett, S.M., Leroi, J.M., Jeffrey, S.W., 1993b. Essential polyunsaturated fatty acids from 14 species of diatom (Bacillariophycea). Phytochemistry 35, 155–161.
Eglinton, G., Hamilton, R.J., 1967. Leaf epicuticular waxes. Science 156, 1322–1335.
Einsele, G., Yan, J., Hinderer, M., 2001. Atmospheric carbon burial in modern lake basins and its significance for the global carbon budget. Glob. Planet. Change 30, 167–195.
Faucon, M.P., Parmentier, I., Colinet, G., Mahy, G., Luhembwe, M.N., Meerts, P., 2011. May rare metallophytes benefit from disturbed soils following mining activity? the case of the Crepidorhopalon tenuis in Katanga (D. R. Congo). Restor. Ecol. 19, 333–343.
Giering, S.L.C., Sanders, R., Lampitt, R.S., Anderson, T.R., Tamburini, C., Boutrif, M., Zubkov, M.V., Marsay, C.M., Henson, S.A., Saw, K., Cook, K., Mayor, D., 2014. Reconciliation of the carbon budget in the ocean's twilight zone. Nature 507, 480–483.
Gombert, P., 2002. Role of karstic dissolution in global carbon cycle. Glob. Planet. Change 33, 177–184.
Gordon, E.S., Goñi, M.A., 2003. Sources and distribution of terrigenous organic matter delivered by the Atchafalaya River to sediments in the northern Gulf of Mexico. Geochim. Cosmochim. Acta 67, 2359–2375.
Grenouillet, G., Buisson, L., Casajus, N., Lek, S., 2011. Ensemble modelling of species distribution: the effects of geographical and environmental ranges. Ecography 34, 9–17.
Guschina, I.A., Harwood, J.L., 2013. Algal lipids and their metabolism. In: Algae for Biofuels and Energy. Springer, Netherlands.
Harwood, J.L., Russell, N.J., 1984. Lipids in Plants and Microbes. George Allen and Unwin, London.
Houghton, R.A., 2007. Balancing the global carbon budget. Annu. Rev. Earth Planet. Sci. 35, 313–347.
Jaffé, R., Wolff, G.A., Cabrera, A.C., Carvajal-Chitty, H., 1995. The biogeochemistry of lipids in rivers from the Orinoco basin. Geochim. Cosmochim. Acta 59, 4507–4522.
Li, W., Dagaut, J., Saliot, A., 1995. The application of sterol biomarkers to the study of the sources of particulate organic matter in the Solo River system and Serayu River, Java, Indonesia. Biogeochemistry 31, 139–154.
Liu, Z., Li, Q., Sun, H., Wang, J., 2007. Seasonal, diurnal and storm-scale hydrochemical variations of typical epikarst springs in subtropical karst areas of SW China: soil CO_2 and dilution effects. J. Hydrol. 337, 207–223.
Liu, Z., Wolfgang, D., 2015. Seasonal, diurnal and storm-scale hydrochemical variations of typical epikarst springs in subtropical karst areas of SW China: soil CO_2 and dilution effects. Sci. Bull. 60, 182–191.
Liu, Z., Wolfgang, D., Liu, H., 2011. Atmospheric CO2 sink: silicate weathering or carbonate weathering. Appl. Geochem. 26, S292–S294.
Liu, Z., Wolfgang, D., Wang, H., 2010. A new direction in effective accounting for the atmospheric CO_2 budget: considering the combined action of carbonate dissolution, the global water cycle and photosynthetic uptake of DIC by aquatic organisms. Earth Sci. Rev. 99, 162–172.
Liu, Z., Zhao, J., 2000. Contribution of carbonate rock weathering to the atmospheric CO_2 sink. Environ. Geol. 39, 1053–1058.
Mahler, B.J., Personne, J.C., Lods, G.F., Drogue, C., 2000. Transport of free and particulate-associated bacteria in karst. J. Hydrol. 238, 179–193.
Marmion, M., Parviainen, M., Luoto, M., Heikkinen, R.K., Thuiller, W., 2009. Evaluation of consensus methods in predictive species distribution modelling. Divers. Distrib. 15, 59–69.
McCallister, S.L., Bauer, J.E., Cherrier, J.E., Ducklow, H.W., 2004. Assessing the sources and ages of organic matter supporting river and estuarine bacterial production: a multiple-isotope ($\delta^{14}C$, $\delta^{13}C$, and $\delta^{15}N$) approach. Limnol. Oceanogr. 49, 1687–1702.
Melnikov, N.B., O'Neill, B.C., 2006. Learning about the carbon cycle from global budget data. Geophys. Res. Lett. 330, 356–360.
MEP, Ministry of Environmental Protection of the People's Republic of China, 2002. Monitoring and Analysis Method of Water and Waste Water, fourth ed. Environmental Science Press, Beijing, China.
Meybeck, M., 1993. Riverine transport of atmospheric carbon: sources, global typology and budget. Water Air Soil Pollut. 70, 443–463.
Meyers, P.A., 1997. Organic geochemical proxies of paleoceanographic, paleolimnologic, and paieoclimatic processes. Org. Geochem. 27, 213–250.
Mezger, D., Pfeiffer, M., 2011. Partitioning the impact of abiotic factors and spatial patterns on species richness and community structure of ground ant assemblages in four Bornean rainforests. Ecography 34, 39–48.
Mohanty, B.P., Bhattacharjee, S., Paria, P., Mahanty, A., Sharma, A.P., 2013. Lipid biomarkers of lens aging. Appl. Biochem. Biotechnol. 169, 192–200.
Montety, V.D., Martin, J.B., Cohen, M.J., Foster, C., Kurz, M.J., 2011. Influence of diel biogeochemical cycles on carbonate equilibrium in a karst river. Chem. Geol. 283, 31–43.
Mortillaro, J.M., Abril, G., Moreira-Turcq, P., Sobrinho, R.L., Perez, M., Meziane, T., 2011. Fatty acid and stable isotope ($\delta^{13}C$, $\delta^{15}N$) signatures of particulate organic matter in the lower Amazon River: seasonal contrasts and connectivity between floodplain lakes and the mainstem. Org. Geochem. 42, 1159–1168.
Nimick, D.A., Gammons, C.H., Parker, S.R., 2011. Diel biogeochemical processes and their effect on the aqueous chemistry of streams: a review. Chem. Geol. 283, 3–17.
O'Reilly, S.S., Szpak, M.T., Flanagan, P.V., Monteysb, X., Murphya, B.T., Jordana, S.F., Allenc, C.C.R., Simpsond, A.J., Mulligana, S.M., Sandrona, S., Kellehera, B.P., 2014. Biomarkers reveal the effects of hydrography on the sources and fate of marine and terrestrial organic matter in the western Irish Sea. Estuar. Coast. Shelf Sci. 136, 157–171.
Poulter, B., Frank, D., Ciais, P., Myneni, R.B., Andela, N., Bi, J., Broquet, G., Canadell, J.G., Chevallier, F., Liu, Y.Y., Running, S.W., Sitch, S., van der Werf, G.R., 2014. Contribution of semi-arid ecosystems to interannual variability of the global carbon cycle. Nature 509, 600–603.
Raymond, P., Bauer, J.E., 2001. DOC cycling in a temperate estuary: a mass balance approach using natural ^{14}C and ^{13}C isotopes. Limnol. Oceanogr. 46, 655–667.
Robinson, N., Cranwell, P.A., Eglinton, G., 1987. Sources of the lipids in the bottom sediments of an English oligo-mesotrophic lake. Freshw. Biol. 17, 15–33.
Rontani, J.F., 2008. Photooxidative and autoxidative degradation of lipid components during the senescence of phototrophic organisms. In: Phytochemistry Research Progress. Nova Science Publishers, New York.
Tue, N.T., Quy, T.D., Hamaoka, H., Mai, T.N., Omori, K., 2012. Sources and exchange of particulate organic matter in an estuarine mangrove ecosystem of Xuan Thuy National Park, Vietnam. Estuaries Coasts 35, 1060–1068.
Viso, A.C., Marty, J.C., 1993. Fatty acids from 28 marine microalgae. Phytochemistry 34, 1521–1533.
Volkman, J.K., 1986. A review of sterol markers for marine and terrigenous organic matter. Org. Geochem. 9, 83–99.
Waterson, E.J., Canuel, E.A., 2008. Sources of sedimentary organic matter in the Mississippi River and adjacent Gulf of Mexico as revealed by lipid biomarker and $\delta^{13}C$ TOC analyses. Org. Geochem. 39, 422–439.
Wigley, T., 1977. WATSPEC: a computer program for determining the equilibrium speciation of aqueous solutions. Br. Geomorphol. Res. Group Tech. Bull. 20, 1–48.
Yunker, M.B., MacDonald, R.W., Veltkamp, D.J., Cretney, W.J., 1995. Terrestrial and marine biomarkers in a seasonally ice-covered Arctic estuary — integration of multivariate and biomarker approaches. Mar. Chem. 49, 1–50.
Yunker, M.B., MacDonald, R.W., Whitehouse, B.G., 1994. Phase associations and lipid distributions in the seasonally ice-covered Arctic estuary of the Mackenzie Shelf. Org. Geochem. 22, 651–669.
Zhang, L., Qin, X., Liu, P., Huang, Q., Lan, F., Ji, H., 2015. Estimation of carbon sink fluxes in the Pearl River basin (China) based on a water–rock–gas–organism interaction model. Environ. Earth Sci. 74, 945–952.
Zheng, B., Zhou, J., Liu, L., Lin, K., Zhu, Y., 2013. The reference condition for eutrophication indictor in the Yangtze River estuary and adjacent—waters response variables. Acta Ecol. Sin. 33, 2780–2789.